Biogeosciences Discuss., 12, 707–749, 2015
www.biogeosciences-discuss.net/12/707/2015/
doi:10.5194/bgd-12-707-2015

Biogeosciences
Discussions
Open Access

Investigating the usefulness of satellite derived fluorescence data in inferring gross primary productivity within the carbon cycle data assimilation system

E. N. Koffi[1,*], P. J. Rayner[2], A. J. Norton[2], C. Frankenberg[3], and M. Scholze[4]

[1]Laboratoire des Sciences du Climat et de l'Environnement (LSCE), UMR8212, Ormes des merisiers, 91191 Gif-sur-Yvette, France
[2]School of Earth Sciences, University of Melbourne, Melbourne, Australia
[3]Jet Propulsion Laboratory, California Institute of Technology, Pasadena, USA
[4]Department of Physical Geography and Ecosystem Science, Lund University, Lund, Sweden
[*]now at: the European Commission Joint Research Centre, Institute for Environment and Sustainability, 21027 Ispra (Va), Italy

Received: 1 December 2014 – Accepted: 15 December 2014 – Published: 13 January 2015

Correspondence to: E. N. Koffi (ernest.koffi@jrc.ec.europa.eu)

Published by Copernicus Publications on behalf of the European Geosciences Union.

Abstract

We investigate the utility of satellite measurements of chlorophyll fluorescence (F_s) in constraining gross primary productivity (GPP). We ingest F_s measurements into the Carbon-Cycle Data Assimilation System (CCDAS) which has been augmented by the fluorescence component of the Soil Canopy Observation, Photochemistry and Energy fluxes (SCOPE) model. CCDAS simulates well the patterns of F_s suggesting the combined model is capable of ingesting these measurements. However simulated F_s is insensitive to the key parameter controlling GPP, the carboxylation capacity (V_{cmax}). Simulated F_s is sensitive to both the incoming absorbed photosynthetically active radiation (aPAR) and leaf chlorophyll concentration both of which are treated as perfectly known in previous CCDAS versions. Proper use of F_s measurements therefore requires enhancement of CCDAS to include and expose these variables.

1 Introduction

The natural terrestrial flux has been identified as the most uncertain term in the global carbon budget (Le Quere et al., 2013). The gross primary productivity (GPP), which is the flux of CO_2 assimilated by plants during photosynthesis, is the input to this system so its variation can significantly contribute to the uncertainties in terrestrial CO_2 fluxes.

Complex systems have been built to reduce the uncertainties in GPP. These systems are either based on up-scaling or atmospheric inverse modeling methods. Up-scaling methods estimate GPP at global scale by establishing relationships between local GPP measurements and environmental variables then using these variables to calculate GPP globally (e.g., Jung et al., 2011; Beer et al., 2010 and references therein). The inverse modeling approach uses CO_2 concentration observations at global scale to constrain the process parameters of carbon models that compute the terrestrial fluxes. This inverse method is an example of Carbon Cycle Data Assimilation Systems (CC-DAS). The CCDAS considered in the present study has two main components:

- A deterministic dynamical model that computes the evolution of both the biosphere and soil carbon stores given an initial condition, forcing and a set of the model process parameters.

- An assimilation system that allows the adjustment of a subset of the state variables, initial conditions and/or process parameters to reduce the mismatch between the model simulations and observations. Usually any prior information on the variables which are adjusted are also taken into account (see e.g., Kaminski et al., 2002, 2003; Rayner et al., 2005, and references therein for the underlying methodology). In the above references the target variables are the process parameters of the Biosphere Energy-Transfer Hydrology (BETHY) model (Knorr, 2000).

Rayner et al. (2005) built such a system around the biosphere model BETHY coupled to atmospheric transport models, see also Kaminski et al. (2013) for an overview on further developments and applications. Koffi et al. (2012) used this CCDAS to investigate the sensitivity of estimates of GPP to transport models and observational networks of CO_2 concentrations. Large differences in GPP in the tropics were found between their estimates and those from either satellite based products or up-scaling methods. Koffi et al. (2012) found significantly larger GPP in the tropics where the parameters of BETHY are weakly constrained due to few CO_2 concentration observations available in this region.

Recent work have inferred plant fluorescence (hereafter F_s) from the Greenhouse gas Observing Satellite (GOSAT; e.g., Frankenberg et al., 2011, 2012; Joiner et al., 2011; Guanter et al., 2012), ENVISAT/SCIAMACHY (Joiner et al., 2012), and MetOp-A/GOME-2 (Joiner et al., 2013). They showed that F_s data are promising for inferring GPP. They found a strong linear correlation between satellite-based F_s and GPP estimated from either up-scaling methods (Jung et al., 2011) or satellite products (MODIS data). The satellite-based F_s data cover large areas of the globe including tropical

BGD
12, 707–749, 2015

zones where estimates from a CCDAS are found to be uncertain. It is worth asking whether such fluorescence data is useful to constrain GPP in the CCDAS framework.

The relationship between fluorescence and photochemistry at leaf level is reasonably well understood. Light energy absorbed by chlorophyll molecules has one of three fates: photosynthesis, dissipation as heat (non-photochemical quenching) or chlorophyll fluorescence. The total amount of chlorophyll fluorescence is only 1 to 2 % of total light absorbed. The spectrum of fluorescence is different to that of absorbed light. The peak of the fluorescence spectrum lies between 650 and 850 nm. Under low light conditions, a negative correlation has been found between fluorescence and photosynthesis light use efficiencies (e.g., Genty et al., 1989; Rosema et al., 1998; Seaton and Walker, 1990; Maxwell and Johnson, 2000; van der Tol et al., 2009). At high light conditions (i.e., high irradiance and moisture stress), a positive correlation has been observed between fluorescence and photosynthesis light use efficiencies (Gilmore and Yamamoto, 1992; Gilmore et al., 1994; Maxwell and Johnson, 2000; Van der Tol et al., 2009). Regarding the water stress, more recently, Jung-See Lee et al. (2012) showed a negative correlation between vapour pressure deficit and F_s.

The cited works show that the link between fluorescence and photosynthesis is complex. Thus, before using fluorescence observations to constrain gross primary productivity in the framework of CCDAS, we need first to ensure that there is a common parameter or set of parameters relevant to both the fluorescence and photosynthesis process models of the CCDAS. So, if there are common parameters, we can assess the sensitivities of GPP and F_s to them. This requires implementing in CCDAS a model that allows computing both fluorescence and photosynthesis. We build such a CCDAS by using the Soil Canopy Observation, Photochemistry and Energy fluxes (SCOPE) model (Van der Tol et al., 2009a, 2014). SCOPE is based on the existing theory of chlorophyll fluorescence and photosynthesis. The photosynthesis scheme of C3 plants uses the formulations of Collatz et al. (1991), while for the C4 photosynthesis pathway, the formulations of Collatz et al. (1992) are considered. In these formulations of the photosynthesis, the maximum carboxylation rate V_{cmax} is a key process parameter. The

BGD
12, 707–749, 2015

fluorescence model is based on the work of Genty et al. (1989), Rosema et al. (1998), and van der Tol et al. (2014). The model is formulated such that the sum of the probabilities of an absorbed photon to result in fluorescence, photochemistry, and heat is unity. Hence, the fluorescence model also utilizes V_{cmax} as a process parameter.

CCDAS operates in two modes (Scholze et al., 2007). The calibration mode that derives an optimal parameter set including posterior uncertainties of the dynamical carbon model (here the biosphere model) by constraining the process parameters of the model with observations. The diagnostic/prognostic (referred hereafter as forward) mode allows deriving the various quantities of interest (e.g., terrestrial carbon fluxes or atmospheric CO_2 concentrations) and their uncertainties. These quantities are calculated from the optimized parameter vector obtained from the calibration step. CCDAS has been widely applied to investigate terrestrial carbon cycling (e.g., Rayner et al., 2005; Scholze et al., 2007) and in particular more recently to (i) estimate the GPP at global scale (Koffi et al., 2012) and (ii) to quantify the uncertainty in the parameters of BETHY by using both CO_2 concentration and flux observational networks (Kaminski et al., 2012; Koffi et al., 2013). To assess the usefulness of satellite based fluorescence data (F_s) to constrain GPP within CCDAS, we first build the forward mode of the CCDAS around the model SCOPE, which is used to investigate the sensitivities of both GPP and F_s to the biochemical parameters as well as environmental conditions.

The work is organized as follows:

In Sect. 2, we describe both the model SCOPE and its coupling with CCDAS and the fluorescence data retrieved from the satellite GOSAT. In Sect. 3, we perform various idealized sensitivity tests to investigate the strength of the relationships between F_s and GPP by using the SCOPE model alone. These tests are performed by studying the sensitivity of GPP and F_s to the biochemical parameters (i.e., V_{cmax} and the chlorophyll content C_{ab}) and the environmental conditions (e.g., short wave radiation R_{in}). The vegetation is characterized by different values of the leaf area index (LAI). In Sect. 4, by using the forward mode of the CCDAS coupled to SCOPE, we compute both F_s and GPP at global scale and results are compared to the GOSAT F_s from June 2009 until

BGD
12, 707–749, 2015

December 2010. The simulations are based on the different settings of LAI, R_{in}, V_{cmax}, and C_{ab} values. In Sect. 5, results are discussed. Finally, conclusions are presented in Sect. 6.

2 Models and data

2.1 Models

2.1.1 SCOPE model

The model SCOPE is a 1-D model based on radiative transfer, micrometeorology, and plant physiology (van der Tol et al., 2009a). Version 1.53 of SCOPE is used in this study with the default version of the biochemical code (referred as fluorescence model choice "0"; van der Tol et al., 2014). SCOPE treats canopy radiative transfer in the visible and infrared and chlorophyll fluorescence, as well as the energy balance. The modules of SCOPE are executed in the following order:

1. A semi-empirical radiative transfer model for incident sun and sky radiation, based on the SAIL model (Verhoef and Bach, 2007). This module calculates the outgoing radiation spectrum (0.4 to 50 µm) at the top of the canopy (hereafter TOC), as well as the net radiation and absorbed photosynthetically active radiation (aPAR) per surface element.
2. A numerical radiative transfer model for thermal radiation generated internally by soil and vegetation, based on Verhoef et al. (2007). This module computes the TOC outgoing thermal radiation and net radiation per surface element, but for heterogeneous leaf and soil temperatures.
3. A biochemistry model for C3 and C4 plants, which allows the computation of quantities relevant for photosynthesis and chlorophyll fluorescence at leaf level. At leaf level, the model calculates a fluorescence scaling factor relative to that of a leaf

BGD
12, 707–749, 2015

Title Page
Abstract Introduction
Conclusions References
Tables Figures
Back Close
Full Screen / Esc
Printer-friendly Version
Interactive Discussion

in low-light, unstressed conditions from absorbed fluxes, canopy and ambient environmental conditions (radiation, temperature, water vapour, CO_2, and O_2 concentrations).

4. A radiative transfer model for chlorophyll fluorescence based on the FluorSAIL model (Miller et al., 2005) that calculates the TOC radiance spectrum of fluorescence over 640–850 nm from the geometry of the canopy and a calculated fluorescence spectrum that is linearly scaled by the leaf level chlorophyll fluorescence scaling factor.

SCOPE uses a canopy structure characterized by a spherical leaf angle distribution as a function of LAI with 60 distributed elementary layers. The geometry of the vegetation is treated stochastically. SCOPE calculates the illumination of leaves with respect to their position and orientation in the canopy. The spectra of reflected and emitted radiation as observed above the canopy in the satellite observation direction are computed. It is worth noting that SCOPE permits variation only in the vertical dimension. Thus, it is valid for vegetation in which variations in the horizontal are smaller than in the vertical dimension. This is maybe a limitation for some natural canopies, especially when coupling to the CCDAS as performed in Sect. 2.1.2. However, the sensitivity of this limitation to the CCDAS results is beyond the scope of this study.

We briefly describe the fluorescence model at leaf level (more detail is given in van der Tol et al., 2009b and van der Tol et al., 2014) with focus on the variables and parameters relevant for the photosynthesis. The model of Faquahar et al. (1980) divides photosynthesis into two main processes: (1) regeneration of the ribulose bisphosphate (RuP2), which depends on the light and (2) the maximum carboxylation rate at RuP2 saturated conditions in the presence of sufficient light. The regeneration of RuP2 for two photosystems (PSII and PSI) gives the link between photosynthesis and fluorescence.

As already mentioned above, the fluorescence model in SCOPE is formulated such that the sum of the probabilities of an absorbed photon to result in fluorescence, pho-

BGD
12, 707–749, 2015

tochemistry, and heat is unity. Following this, the fluorescence Φ_{Ft} from a single leaf is calculated over the spectrum window of 640–850 nm as follows:

$$\Phi_{Ft} = \Phi_{Fm}(1 - \Phi_p) \tag{1}$$

Where Φ_{Fm} is the fluorescence yield and computed as follows:

$$\Phi_{Fm} = \frac{K_f}{(K_f + K_d + K_n)} \tag{2}$$

With

$$K_n = (6.2473x - 0.5944)x \tag{3}$$

Where x stands for the degree of light saturation and defined as:

$$x = 1 - \frac{\Phi_p}{\Phi_{p0}} \tag{4}$$

Φ_p and Φ_{p0} (given by the following expressions) stand for the fractions of actual and dark photochemistry yields, respectively:

$$\Phi_{p0} = \frac{K_p}{(K_f + K_d + K_p)} \tag{5}$$

K_f is the rate constant for fluorescence and sets to 0.05.
K_p is the rate constant for photochemistry with a value of 4.0.
K_d, with a value of 0.95, is the rate constant for thermal deactivation at Φ_{Fm}.

$$\Phi_p = \Phi_{p0}\frac{J_a}{J_e} \tag{6}$$

BGD
12, 707–749, 2015

J_a and J_e stand for the actual and potential electron transport rates, respectively. J_a is the electron transport rate used for gross primary productivity (GPP). van der Tol et al. (2014) used Pulse-Amplitude fluorescence measurements to derive an empirical relation between the efficiencies of photochemistry and fluorescence. This relationship was derived after analysing the response of non-photochemical quenching (NPQ) in plants to light saturation. The formulations of GPP in SCOPE follow that of Collatz et al. (1991) and Collatz et al. (1992) for C3 and C4 plants, respectively. The potential electron transport rate J_e is related to the rate of absorbed photons (or absorbed photosynthetically active radiation, i.e., aPAR), hence to the visible radiation. The fluorescence is linearly related to the short wave (visible) radiation, while it is related to V_{cmax} mainly when the gross primary productivity GPP is limited by the carboxylation enzyme Rubisco and the capacity for the export or the utilization of the products of photosynthesis.

The total top-of-canopy fluorescent radiance is obtained by a summation of the fluorescence Φ_{Ft} (Eq. 1) from each of the leaves over all layers and orientations, taking into account the probabilities of viewing sunlit and shaded components. The model then calculates radiation transport in a multilayer canopy as a function of the solar zenith angle and leaf orientation to simulate fluorescence in the direction of satellite observation (Van der Tol et al., 2009a).

Leaf biochemistry affects reflectance, transmittance, transpiration, photosynthesis, stomatal resistance, and chlorophyll fluorescence. Reflectance and transmittance coefficients, which are a function of C_{ab} are calculated by following the PROSPECT model (Jacquemoud and Baret, 1990). Two excitation fluorescence matrices (EF-matrices) representing fluorescence from both sides of the leaf are computed. The matrices convert a spectrum of aPAR into a spectrum of fluorescence. Details on the radiative transfer model of the fluorescence at the TOC level are given in Van der Tol et al. (2009a).

2.1.2 Coupling SCOPE to CCDAS

Within CCDAS we replace the radiative transfer and photosynthesis schemes of BETHY with their corresponding schemes from SCOPE and add the fluorescence model of SCOPE. The spatial resolution, vegetation characteristics as well as the meteorological and phenological data of BETHY are used to force SCOPE. The spatial resolution is $2^\circ \times 2^\circ$ with 3462 land grid points for the globe. CCDAS uses 13 plant functional types (PFT) based on Wilson and Henderson-Sellers (1985). A grid cell can contain up to three different PFTs, with the amount specified by their fractional coverage.

2.2 Data

2.2.1 GOSAT fluorescence data

Frankenberg et al. (2011, 2012), Joiner et al. (2011), and Guanter et al. (2012) have published maps of F_s from GOSAT (Kuze et al., 2009). The retrieval measures terrestrial emission at the frequencies of solar Fraunhofer lines (gaps in the solar spectrum). Chlorophyll fluorescence is the main contributor to emissions at these frequencies. GOSAT carries a Fourier Transform Spectrometer (FTS) measuring with high spectral resolution in the 755–775 nm range, which allows resolving individual Fraunhofer lines overlapping the fluorescence emission. The method described in Frankenberg et al. (2011) makes use of two spectral windows centered at 755 and 770 nm to derive F_s. Results from the line centered around 755 nm for the period June 2009 to December 2010 are used in this study. The fluorescence data we are using are monthly means mapped onto $2^\circ \times 2^\circ$ spatial resolution at global scale. The fluorescence product includes uncertainties.

BGD
12, 707–749, 2015

2.2.2 Data relevant for models

The input data for the models we are using are of four main kinds: (i) the data for the radiative transfer modules of SCOPE, (ii) the data characterizing the environmental conditions (i.e., meteorological and short and long wave radiation) relevant for both the radiative transfer and biochemistry models, (iii) the leaf area index (LAI) for the radiative transfer and biochemistry models, and (iv) the process parameters of the biochemistry models.

The model SCOPE requires incident radiation at the top-of-canopy as input. To take into account the atmospheric absorption bands properly, this data is needed at high resolution. The spectra of sun and sky fluxes at the top of the canopy are obtained from the atmospheric radiative transfer model MODTRAN (Berk et al., 2000). MODTRAN was run for 16 atmospheric situations representative of different regions (Verhoef et al., 2014). We use 4 types of these generated atmospheres. They are tropical atmosphere for the tropical zones, winter and summer atmospheres for high and middle latitudes. In addition, we have at our disposal data for an atmosphere which is representative of the whole globe (hereafter "standard atmosphere"). We have tested the sensitivity of F_s and GPP to these four types of atmospheres. Results show only residual differences between the inferred F_s and GPP. We consider the standard atmosphere for the idealized tests (Sect. 4.1) and the seasonal atmosphere for the simulations at global scale by using the CCDAS (Sect. 4.2).

The system needs forcing data to drive SCOPE within the CCDAS framework. Monthly observed climate, incident radiation, and fractional soil moisture for the period 2009–2010 are used (Weedon et al., 2011). The LAIs are obtained from BETHY simulation.

The main parameters that affect both the photosynthesis and fluorescence schemes are given in Table 1. The parameters are of two kinds: parameters that are PFT-specific (e.g., V_{cmax} and C_{ab}) and global parameters. Prior and optimized values of V_{cmax} obtained by Koffi et al. (2012) are shown. The chlorophyll content C_{ab} is related to the

BGD
12, 707–749, 2015

nitrogen content of the leaf which itself is linked to the maximum rate of carboxylation through the proteins of the Calvin Cycle and the thylakoids. Some investigators have related the photosynthetic capacity of leaves of some specific plants to their nitrogen content (e.g., Evans, 1989; Kattge et al., 2009; Houborg et al., 2013). Other workers have derived some empirical relationships between the nitrogen content and the chlorophyll content (e.g., Shaahan et al., 1999; Van den Berg and Perkins, 2004; Ghasemi et al., 2011). Since the current version of the model SCOPE does not include the nitrogen scheme of a leaf, we first use the same value of chlorophyll content C_{ab} for all 13 PFTs. As a second step, C_{ab} values for each of the 13 PFTs are optimized so that the simulated F_s reproduces the main spatial characteristics of observed F_s.

3 Experimental set ups

3.1 Idealized tests

We carry out some idealized sensitivity tests by using the SCOPE model alone. We investigate the sensitivity of F_s and GPP to biochemical parameters V_{cmax} and C_{ab}, environmental variables (temperature, vapour pressure, etc), visible radiation, and LAI. We assume throughout the following sections the concentrations of both CO_2 and O_2 at the interface of the canopy to be constant. We will focus our discussions on the assessment of the sensitivity of the simulated F_s and GPP to V_{cmax}, C_{ab}, and the short wave radiation.

We present a spectrum of simulated fluorescence for C3 and C4 plants in Fig. 1. Two peaks in the simulated fluorescence spectrum are shown at 680 and 725 nm. In agreement with van der Tol et al. (2009a), C4 plants exhibit larger F_s than C3 plants over the wavelength range 625 to 755 nm. These differences are amplified around the two peaks. We are using as observations the GOSAT satellite derived $F_{s,}$ which retrieved F_s around 755 nm. Therefore, the simulated fluorescence in this study corresponds to the F_s value at this wavelength. In Fig. 1, this is around 1.2 $W\,m^{-2}\,\mu m^{-1}\,sr^{-1}$.

BGD
12, 707–749, 2015

For all the idealized tests presented hereafter, we use 8 values of LAI: 0.1, 0.5, 1, 2, 3, 4, 5, and 6. We select these values to be able to characterize different types of canopy from sparse to dense vegetation. Also, the pressure, the temperature, and the water vapour pressure are set to 1000 hPa, 25 °C, and 10 hPa, respectively. The carbon dioxide (CO_2) and the oxygen (O_2) concentrations are set to 355 ppm and 210 × 10^3 ppm, respectively. We consider the value of the simulated fluorescence F_s from SCOPE at 755 nm.

- To investigate the sensitivity of F_s and GPP to the maximum carboxylation capacity V_{cmax}, we choose V_{cmax} values ranging from 10 to 250 µmol (CO_2) m^{-2} s^{-1} every 10 µmol m^{-2} s^{-1}. In addition, two small V_{cmax} values of 0.5 and 5 µmol m^{-2} s^{-1} are considered.

- To study the sensitivity of F_s and GPP to the chlorophyll content AB (C_{ab}) we select C_{ab} values that span 10 to 80 µg cm^{-2} range every 5 µg cm^{-2}. Additionally, a small C_{ab} value of 1 µg cm^{-2} is considered.

- To assess the sensitivity of the F_s and GPP to the short wave radiation (R_{in}) at the top of the canopy, we select R_{in} values that range from 100 W m^{-2} to 1300 W m^{-2} every 100 W m^{-2}. We add small values of 1, 5, 10, 25, 50, and 75 W m^{-2}.

- Finally, to investigate the diurnal variations, we simulate F_s and GPP by using the short time series of half hourly data over 16–20 June 2006 over a canopy located at 52.25 deg. latitude and 5.69 deg. longitude in the Netherlands described in Su et al. (2009). Unfortunately, we do not have observed F_s and GPP for this period.

3.2 CCDAS simulations

Since the idealized tests may give a partial picture of the relationship between F_s and GPP, we use the CCDAS built around SCOPE to perform additional sensitivity tests by using actual meteorological, radiation, and phenological data over 2009–2010. The

BGD
12, 707–749, 2015

Investigating the usefulness of satellite derived fluorescence data

E. N. Koffi et al.

relationship between F_s and GPP is then investigated along with V_{cmax} and C_{ab}. We make simulations of F_s and GPP by using prior values of V_{cmax} and their optimized values from Koffi et al. (2012). We also carry out simulations by using a constant value of C_{ab} for all the 13 PFTs and a set of C_{ab} values for each of them. We perform 4 experiments (i.e., S1 to S4), which are summarized in Table 2. The experiments S1 and S3 use a constant value of C_{ab} for all the 13 PFTs, while simulations S2 and S4 consider C_{ab} to be PFT dependent (C_{ab} values are reported in Table 1). The experiments S1 and S2 consider the prior values of V_{cmax}, while S3 and S4 their optimized values. The differences between S1 and S3 or between S2 and S4 give the sensitivity of F_s and GPP to V_{cmax}. The differences between S1 and S2 or between S3 and S4 mainly give the sensitivity of F_s to C_{ab}.

The CCDAS simulates hourly F_s and GPP for one representative day in a month. Since the computation of fluorescence is time consuming, we compute both F_s and GPP only at 12 h local time, i.e., around the time of their peaks during a sunny day. For the simulated F_s, the computations are assigned to the 15th day of the month. We also neglect the energy balance scheme in SCOPE which weakly affects F_s.

4 Results

4.1 Idealized sensitivity tests using SCOPE

The results of these idealized sensitivity tests for the various LAI values are summarized in Figs. 2 and 3. For clarity, results from C3 plant are discussed. Then, some conclusions are given for C4 plant.

4.1.1 Sensitivity of F_s and GPP to biochemistry parameters

As expected, both the fluorescence F_s and GPP increase with the increase of LAI (Fig. 2). However, a weak sensitivity is found for LAI values greater than 4. As an illustration for the increase, for $V_{cmax} = 50\,\mu\mathrm{mol\,m^{-2}\,s^{-1}}$, F_s values of 0.5 and

$1.25\,\mathrm{W\,m^{-2}\,\mu m^{-1}\,sr^{-1}}$ are found for LAI of 0.5 and 2, respectively (Fig. 2a). The fluorescence slightly increases with an increase of V_{cmax}. The sensitivity is relatively large for V_{cmax} less than $70\,\mathrm{\mu mol\,m^{-2}\,s^{-1}}$. Then, F_s remains almost constant for V_{cmax} higher than $125\,\mathrm{\mu mol\,m^{-2}\,s^{-1}}$ (Fig. 2a). As an illustration, for LAI = 2, the largest increase is of only 50 % of F_s for V_{cmax} between 10 and $70\,\mathrm{\mu mol\,m^{-2}\,s^{-1}}$. Under the studied configurations F_s increases with V_{cmax} when the GPP is controlled by the carboxylation enzyme Rubisco, and remains almost constant when the electron transport rate is activated.

GPP monotonically increases as V_{cmax} increases with large sensitivity for small V_{cmax} (less than $75\,\mathrm{\mu mol\,m^{-2}\,s^{-1}}$), then it becomes weakly sensitive for large values of V_{cmax} (Fig. 2b). A moderate positive correlation is found between F_s and GPP for V_{cmax} less than $125\,\mathrm{\mu mol\,m^{-2}\,s^{-1}}$. Then, for larger V_{cmax} (i.e., $125\,\mathrm{\mu mol\,m^{-2}\,s^{-1}}$), a very weak negative correlation between F_s and GPP is obtained. The reason for this weak negative correlation is that F_s slightly decreases for large V_{cmax}, while GPP even limited by the carboxylation enzyme Rubisco still slightly increases (Fig. 2a and b). In fact, the value of irradiance at which the fluorescence at leaf level Φ_{Ft} (Eq. 1) or F_s peaks increases with the increase of V_{cmax}. Thus, for the case presented in Fig. 2a with the short wave radiation R_{in} of $500\,\mathrm{W\,m^{-2}}$, the peak of F_s occurs at about $V_{cmax} = 200\,\mathrm{\mu mol\,m^{-2}\,s^{-1}}$.

In the current version of the fluorescence model in SCOPE, the concentration of chlorophyll C_{ab} is set as a parameter and it is linked to F_s through the transmittance and reflectance of the leaves. Figure 2c portrays the variations of F_s as a function of C_{ab} and for various LAIs. For a given LAI, F_s increases with C_{ab} with large sensitivity for C_{ab} less than $20\,\mathrm{\mu g\,cm^{-2}}$. For larger C_{ab} values (i.e., $> 50\,\mathrm{\mu g\,cm^{-2}}$), F_s remains almost constant with a tendency to slightly decrease as C_{ab} increases. For a given C_{ab}, the variance in F_s due to the LAI can be significant.

Figure 2d displays GPP as a function of C_{ab} (Fig. 2d). Except for small values of C_{ab} (less than $5\,\mathrm{\mu g\,cm^{-2}}$), GPP is not sensitive to C_{ab}. The very weak sensitivity of GPP to C_{ab} comes from the impact of the chlorophyll content on the transmittance and reflectance at the top of the canopy when computing the aPAR.

4.1.2 Sensitivity of F_s and GPP to short wave radiation

For a given LAI, both F_s and GPP increase with the top of canopy short wave radiation (R_{in}) (Fig. 2e and f). Thus, a strong positive linear correlation is obtained between F_s and R_{in} (Fig. 2e), while a non-linear (i.e., curvilinear) relationship is obtained between GPP and R_{in} (Fig. 2f). For large R_{in}, GPP increases with a slower rate indicating that the photosynthesis is limited by the carboxylation enzyme Rubisco. For the selected values of LAI, large variance is found between F_s and R_{in} (Fig. 2f). We also investigate the relationship between the simulated aPAR and both computed F_s and GPP (not shown). A very strong linear relationship between F_s and aPAR is obtained. This relationship is less sensitive to the LAI as it is for the relation between F_s and R_{in} (as shown in Fig. 2e). GPP shows similar variations with aPAR as it does with the short wave radiation in Fig. 2f.

Finally, the sensitivities of F_s and GPP to aPAR for various V_{cmax} are also investigated (Fig. 3). A strong linear relationship between F_s and aPAR is obtained with slopes which are less sensitive to the values of V_{cmax} (Fig. 3a). Also, results clearly show that the sensitivity of F_s to V_{cmax} increases with the increase of aPAR, with almost no sensitivity for low values of aPAR ($< 250\,\mathrm{W\,m^{-2}}$). However, even with large values of aPAR, the sensitivity of F_s to V_{cmax} remains small. As expected, a curvilinear relationship is found between GPP and aPAR with large variance in this relation for the selected V_{cmax} (Fig. 3b).

The conclusions found from C3 plant relevant for the sensitivity of both F_s and GPP to the input variables (V_{cmax}, C_{ab}, and R_{in}) are valid for C4 plant (not shown). However, the amplitude of these sensitivities is slightly larger for C4 plant.

4.1.3 Simulations of in situ measurements

The time series of both simulated F_s and GPP for 16–20 June 2006 are presented in Fig. 4. As expected, there is a strong correlation between aPAR and the short wave radiation R_{in} (Fig. 4b), hence we discuss the results as a function of the observed R_{in}.

BGD
12, 707–749, 2015

The temporal variations of F_s and GPP mainly follow that of R_{in}. Particularly, the variations of F_s mirror that of R_{in}, showing that the variance in F_s due to the temperature is low in this case study (Fig. 4a). At high irradiance GPP shows limitation by the carboxylation enzyme Rubisco, peaking early in the day whereas F_s follows R_{in} throughout the day. The small variations in GPP at certain episodes can be explained by the temporal variations of both the temperature and the vapour pressure (Fig. 4a). Note that V_{cmax}, C_{ab}, and LAI are set constant during this period. Consequently, for this case study, the short wave radiation (hence aPAR) is the main driver of the relationship between F_s and GPP. A curvilinear relation is obtained between GPP and F_s. However, a relatively strong linear correlation coefficient of 0.9 is derived. This suggests that F_s is a good constraint of GPP even if it does not directly constrain V_{cmax}.

In summary, these idealized tests clearly show that the fluorescence F_s is more sensitive to C_{ab}, while GPP is more sensitive to V_{cmax} and both quantities are strongly sensitive to the short wave radiation (or aPAR). However, GPP is limited by the carboxylation enzyme Rubisco for large values of short wave radiation (or aPAR). Consequently, in this case the relationship between F_s and GPP mainly driven by the short wave radiation (or aPAR) is curvelinear. The part of the variance in this relationship due to the GPP can be explained by V_{cmax} and environment conditions, while the variance in F_s is mainly due to C_{ab} and possibly to the geometrical parameters (i.e., solar zenith angle and observation zenith angle) used in the retrieval of F_s.

4.2 CCDAS Simulations

To assess the relationship between F_s and GPP at global scale, we perform the four experiments described in Table 2. The results of these simulations are discussed along with the satellite-based F_s. We first analyze the correlations between the simulated quantities and also the correlations between these simulations and the satellite based F_s. Second, their mean spatial patterns are discussed and finally, the time series of their global and regional means as well as their zonal averages are discussed.

4.2.1 Correlations between F_s and GPP

For the discussion of the time series of modeled F_s and GPP at each CCDAS land pixel and the corresponding observed F_s we analyze only pixels for which we have at least one year satellite-based F_s data. Moreover, we consider only the time series of these quantities for which the satellite-based F_s data show consecutive values greater than zero. Overall, the simulated F_s and GPP agree reasonably well with the satellite-based F_s for most pixels. The seasonality of the satellite derived F_s is reasonably well reproduced by both the simulated F_s and GPP as illustrated in Fig. 5. In accordance with the idealized tests, the amplitudes of the satellite derived F_s can be better fitted by appropriate values of C_{ab} (Fig. 5a), while the simulated GPP is only weakly sensitive to small C_{ab} values as discussed in Sect. 4.1. As expected, the amplitudes of the simulated GPP are strongly sensitive to V_{cmax} (Fig. 5b).

We have computed the Pearson correlation coefficient between the time series of satellite-based F_s and modelled F_s and GPP at each pixel. For each pixel, we consider only the pair of data for which the satellite-based F_s is greater than or equal to zero. At most, 18 pairs of data are available for each pixel. We treat only pixels with at least 14 data points. Thus, a linear correlation is significant at least 10 % of level of significance for Pearson coefficient greater than 0.43. For about half of the 3462 land pixels of CCDAS, the linear correlation coefficient between the satellite-based F_s and either simulated F_s or GPP is small. For these latter pixels, we have analyzed the time series of the satellite-based F_s (with their uncertainty) jointly with the simulated F_s and GPP together with the aPAR as representative of the short wave radiation. For brevity sake, we only enumerate the different cases without quantification since this does not add anything valuable to our demonstration in the current study. We have cases for which:

- The peaks in simulated quantities (i.e., F_s and GPP) lag the satellite-based F_s peak by at least one month. Other cases show opposite behavior.

BGD
12, 707–749, 2015

- The simulated F_s remain almost constant, while the satellite-based F_s show a weak seasonality. Such cases predominantly occur in the tropics.
- The satellite-based F_s are larger ($> 2\,W\,m^{-2}\,\mu m^{-1}\,sr^{-1}$) than modeled F_s (around $1.2\,W\,m^{-2}\,\mu m^{-1}\,sr^{-1}$). Such cases are mainly obtained in the tropics and for the PFT 1 (i.e., tropical broadleaved evergreen tree).
- The simulated F_s are larger than satellite based F_s. Such cases are mainly obtained from the PFT 9 (i.e., C3 grass).
- The satellite-based F_s show some unexpected peaks during period where they are not expected and hence not modeled.

Second, we investigate the correlations between the simulated quantities (F_s, GPP, and aPAR) at regional scales by using our best set up (i.e., experiment S4 in Table 2). We then assess the correlations between the simulated quantities (F_s, GPP, and aPAR) and between simulated quantities and the satellite-based F_s. We select data at each pixel such that the satellite-based F_s is greater or equal to zero and CCDAS land pixel (i.e., the maximum fraction of coverage of the dominant PFT of the pixel) is greater than zero. Data from June 2009 to end of 2010 are analyzed. We also give information about the dominant PFT of the pixels over the studied time period. To sample only over grid cells which are dominated by only one PFT, we consider only pixels for which the dominant PFT has a fraction of coverage greater than 50 %. Correlations are computed for the global and regional (Northern Hemisphere, tropics, and Southern Hemisphere) regions and over the studied period. The results at global scale are shown in Fig. 6. A strong linear correlation is found between the computed F_s and aPAR. This relation is weakly sensitive to the PFTs (Fig. 6a). In contrast, the relationship between GPP and aPAR is PFT dependent (Fig. 6b). A good linear relationship between computed GPP and simulated F_s is obtained and again the slopes of this relationship are PFT dependent (Fig. 6c). The correlation coefficient R derived from GPP as a function of F_s value is around 0.8.

BGD
12, 707–749, 2015

The model SCOPE simulates quite well the observed F_s (Fig. 6d). However, large observed F_s ($> 2\,W\,m^{-2}\,\mu m^{-1}\,sr^{-1}$) are not simulated. Such large observed F_s mainly occur in the tropics. This result points out that short wave radiation used in the CCDAS simulations may be smaller than actual values. The contribution of chlorophyll content C_{ab} is low since the assigned value in tropics is already large ($40\,\mu g\,cm^{-2}$) and as shown by the idealized tests, the simulated fluorescence F_s remains almost constant for C_{ab} value larger or equal to $40\,\mu g\,cm^{-2}$ (Fig. 2c). The correlation coefficient between modelled GPP and satellite-based F_s is 0.70 (Fig. 6e). This rises to 0.8 when we aggregate both quantities to $4° \times 4°$ in agreement with Frankenberg et al. (2011). Finally, as expected, a relatively good correlation is found between aPAR and satellite based F_s (Fig. 6f).

Correlations are found to be larger between simulated quantities and satellite-derived F_s in the Northern Hemisphere and moderate in the tropics and lower in the Southern Hemisphere (not shown).

4.2.2 Mean spatial patterns of F_s and GPP

We compute the mean annual patterns of the satellite-based F_s and simulated F_s and GPP for 2010. We discuss the simulated quantities by using the experiments S3 (i.e., optimized V_{cmax} and constant C_{ab} for all the 13 PFTs) and S4 (optimized V_{cmax} and C_{ab} PTF-specific) (See Table 2).

Figure 7 displays the annual mean observed and simulated $F_{s,}$ as well as simulated GPP. Figure 7a shows the satellite based F_s. Figure 7b displays the modelled F_s by using constant C_{ab} for the 13 PFTs (experiment S3; Table 2), while Fig. 7c presents model results of F_s for C_{ab} PTF-specific (experiment S4). Figure 7d exhibits the simulated GPP by using both C_{ab} PFT-specific and optimized V_{cmax} (experiment S4). The model can reasonably reproduce the mean spatial patterns of the satellite-based F_s with an appropriate choice of C_{ab} values for each of the 13 PFTs (Fig. 7a and c). The model with constant C_{ab} cannot reproduce the locations of maximum observed F_s (Fig. 7a and b).

BGD
12, 707–749, 2015

Despite the good correlation, the computed F_s with PFT-specific C_{ab} (Table 2) underestimates the satellite-based data (Fig. 7a and c). Some of this mismatch corresponds to unlikely locations for satellite-derived F_s, e.g. central Australia.

A good agreement between the spatial patterns of GPP and satellite-based F_s is found (Fig. 7a and d). Overall, we have a co-occurrence of hot spots of observed F_s and simulated F_s and GPP. Moreover, maximum simulated F_s coincides with maximum APAR (not shown).

The small sensitivity of simulated F_s to V_{cmax} suggests it may be difficult to use observations of F_s to constrain it. We can test this in a more realistic context by comparing the differences between simulated F_s for prior and optimized values of V_{cmax}. If differences are large compared to uncertainties in the observation then F_s observations would allow constraining V_{cmax}. We compute the differences between simulated F_s by using prior V_{cmax} (experiment S2 in Table 2) and optimized V_{cmax} (experiment S4). Then, we normalize these differences by the uncertainties in satellite based F_s. The derived root mean square over year 2010 at pixel level can reach up to 67 % of the observed uncertainties, but the global average is only 6 %. This suggests that F_s measurements can only weakly constrain V_{cmax} within the current CCDAS.

4.2.3 Global and regional means of F_s and GPP

We compute the global and regional (i.e., Northern Hemisphere [30°–90° N], Tropics [30° S–30° N] and Southern Hemisphere [90° S–30° S]) means at each month of the year and over June 2009 to December 2010 over land pixels. Results of both simulated F_s and GPP from our best experimental set up (i.e., optimized V_{cmax} with C_{ab} PTF-specific; experiment S4 in Table 2) are discussed. The results show a reasonably good agreement between satellite-based F_s and both simulated F_s and GPP in terms of seasonality (Fig. 8). However, on average, the simulated quantities peak one month earlier than the peak of the satellite-based F_s (Fig. 8a). In the Northern Hemisphere, satellite-based F_s peaks in July, while simulated F_s reaches its maximum in June (Fig. 8b). The seasonality at global scale is dominated by the North Hemisphere (Fig. 8a and b). In

BGD
12, 707–749, 2015

the tropics, there is no significant seasonality in the satellite-based F_s, which is also reproduced by the model (Fig. 9c). In the Southern Hemisphere, the satellite-based F_s peaks in January, while modeled peaks in December (Fig. 8d). This weak seasonality shift in the CCDAS simulations is driven by the visible radiation at the top of the canopy (or aPAR) and LAI.

Quantitatively, the mean values of the simulated F_s are slightly smaller than that of satellite-based (about 93 %) in the North hemisphere and the tropics. Since the above-mentioned regions dominated the amplitude of F_s, a good agreement between simulated and satellite-based F_s is consequently found at global scale. The simulated F_s in the Southern Hemisphere is about 1.47 times the value of satellite-based F_s. The main differences occur in Australia where the relatively large values of modeled F_s are not shown in the satellite-based F_s data (See Fig. 7a and c).

The zonal averages over the CCDAS land pixels of the satellite-based F_s and the simulated quantities (F_s and GPP) are shown in Fig. 9. A good agreement is found between the latitudinal variations of the satellite-based F_s and the simulated F_s by using the C_{ab} PFT-specific (Fig. 9). Also, a good agreement is obtained between the satellite-based F_s and the GPP (Fig. 9). All three quantities show maxima in the tropics and around 45° N. Simulated F_s values are smaller than the satellite-based F_s in the tropics. Between −15 and −45°, the differences are mainly due to C4 grass for which both the model's V_{cmax} and C_{ab} are apparently small. Around −35° latitude, the differences are mainly due to the fact that the model simulates a large F_s signal over Australia, while the satellite-based F_s shows only a small F_s signal. This discrepancy might be explained by the uncertainty in the LAIs set to the evergreen shrub in the CCDAS in this area. Apparently, the LAIs in the CCDAS seem larger than expected values that give satellite based F_s measurements.

In summary, the agreement between simulated and observed F_s is better as we move to larger and larger scales.

BGD
12, 707–749, 2015

5 Discussions and concluding remarks

The first global maps of F_s retrieved from GOSAT measurements show promise in estimating the terrestrial gross photosynthetic uptake flux of CO_2 (GPP) (Frankenberg et al., 2011; Joiner et al., 2011). We have investigated the usefulness of these data in constraining GPP in the framework of CCDAS. We have augmented CCDAS with SCOPE, which allows the calculation of GPP and F_s at leaf and canopy levels. In CCDAS, the relationship between F_s and GPP is mediated by process parameters, principally the maximum carboxylation capacity (V_{cmax}). Parameters not currently included in CCDAS such as the chlorophyll content (C_{ab}) of the leaves also affects the observed fluorescence and so constitutes a nuisance variable in an assimilation of F_s into CCDAS. We first calculate the sensitivity of F_s and GPP in the standalone SCOPE model to a series of parameters, inputs or nuisance variables. F_s and GPP both respond strongly to incoming radiation suggesting that, insofar as this input is uncertain, F_s can provide a useful constraint. This uncertainty is currently not considered in the CCDAS under study.

The relationship between V_{cmax} and F_s is more complicated and weaker suggesting that the conventional approach of using model parameters to mediate information from F_s to GPP is unlikely to work. C_{ab} also controls F_s while it has little impact on the desired GPP making it a classical nuisance variable. Any model seeking to use F_s should therefore account for chlorophyll concentration.

The simulations of CCDAS confirm the results from the idealized tests. Thus, the relationship between the simulated GPP and computed F_s is again found to be mainly controlled by the short wave radiation or aPAR. The analyses also show that a robust linear relationship between F_s and GPP can be inferred for each PFT. This result is in agreement with the finding of Guanter et al. (2012).

We compared observed F_s with simulated F_s and GPP. The analyses showed a need to select meaningful values for the chlorophyll content C_{ab} for each of the 13 PFTs to better reproduce the satellite-based F_s. The use of PFT-specific C_{ab} allows a better

BGD
12, 707–749, 2015

reproduction of the satellite-based F_s, with good co-location of the hot spots. Timing of large-scale means is also good but this breaks down at pixel level. The global and regional as well as the zonal averages of the simulated quantities (F_s and GPP) are in good agreement with the satellite-based F_s. On average, the peaks in simulated F_s and GPP lag by one month the peaks in satellite-derived F_s in both southern and Northern Hemispheres. The simulated quantities are found to be better correlated to the satellite based F_s when integrating the data at regional scales. More particularly, we found a significant linear correlation between simulated GPP and observed F_s, but a large scatter within the data is obtained. Such a variance can be attributed partly to the type of vegetation.

The study suggests some prospects for the use of satellite-based F_s to constrain GPP. While we found a good correlation between the global and regional and zonal averages of simulated quantities and satellite-based F_s, we do not find a common process parameter that propagates the information from the fluorescence to the GPP. Indeed, the relationship between GPP and satellite based F_s is mainly driven by the short wave radiation or aPAR. Consequently, the mechanistic formulations of both F_s and GPP under study do not allow us to constrain GPP through V_{cmax}.

Recent investigations by Zhang et al. (2014) show a very strong sensitivity of F_s to V_{cmax} at in situ level using SCOPE version 1.52. Zhang et al. (2014) found about 4 times our sensitivity of F_s to V_{cmax} in the range of 20–200 $\mu mol\,m^{-2}\,s^{-1}$ as shown in our Figs. 2 and 3. We have modified our experiments to bring them closer to those of Zhang et al. (2014). First, Zhang et al. (2014) calculate F_s at 740 vs. 755 nm in this study. Second Zhang et al. (2014) average their calculations from 09:00–12:00 local time, while we sample at 12:00. Results show that:

- The sensitivity of F_s to V_{cmax} is slightly larger at 740 nm than 755 nm and the difference increases with aPAR. However, as an example, for a relatively large aPAR (1400 $W\,m^{-2}$), F_s at 740 nm is only 25 % higher than F_s at 755 nm.
- The averaging period makes little difference to the sensitivity.

BGD
12, 707–749, 2015
Investigating the usefulness of satellite derived fluorescence data
E. N. Koffi et al.

– Optimal choices of temperature and LAI produce a sensitivity about 2/3 that shown in Zhang et al. (2014). We would expect to reproduce their results so these differences remain under investigation.

On the other hand, the results clearly show the good correlation between aPAR and both the fluorescence F_s and GPP, which support previous investigations. This both points to a simpler application of F_s in constraining GPP and a problem with the foregoing study. aPAR is an external forcing for BETHY which is taken to be well-known. Errors in forcing (like other nonparametric errors) are added to the observational error in CCDAS (Rayner et al., 2005), but the observations are unable to improve estimates of forcing. The parametric studies above hence miss a potential role of the F_s measurements in constraining GPP even if they cannot constrain process parameters.

Monteith (1972) proposed an empirical linear relation between GPP and aPAR which has been widely used by the satellite community to derive the GPP. The slope of this relationship is the efficiency (ε_p) with which the absorbed radiation is converted to fixed carbon. ε_p varies with physiological stress. We have seen a strong linear relationship between the fluorescence F_s and aPAR. Thus, the GPP is directly linked to F_s by the ratio $\varepsilon_p/\varepsilon_f$. Such an approach is described in a recent report of Berry et al. (2013). This approach would be easier to implement. It could be combined with other pertinent data for GPP (e.g., CO_2 or Carbonyl sulfide (COS) concentration) within a simplified CCDAS. This approach will be applied in a future study.

This study also shows a very weak sensitivity of GPP to the chlorophyll content (C_{ab}) present only for small C_{ab}. This probably does not reflect reality. In the current version the SCOPE model, C_{ab} and V_{cmax} are independent parameters, but in reality they are correlated. In fact, C_{ab} is related to the nitrogen content of the leaf which itself is linked to V_{cmax} (e.g., Kattge et al., 2009; Houborg et al., 2013). In addition, the nitrogen content of the leaf affects both the leaf transmittance and reflectance which influences the aPAR and then the GPP. Thus, through the inclusion of a nitrogen scheme a more apparent link between C_{ab} and GPP and greater sensitivity could be achieved.

BGD
12, 707–749, 2015

6 Conclusions

We have investigated the usefulness of satellite derived fluorescence data to constrain GPP within CCDAS. We have coupled the SCOPE model to CCDAS to allow computing both fluorescence F_s and GPP. We have assessed the sensitivity of both F_s and GPP to the environmental conditions at the interface of the canopy (short wave radiation and meteorological variables) and the biophysical parameters (V_{cmax} and C_{ab}) by using idealized and CCDAS simulations. Our results show:

- As expected, GPP is strongly sensitive to V_{cmax}, while F_s is more sensitive to C_{ab} and only weakly sensitive to V_{cmax}.
- The relationship between simulated F_s and GPP is mainly driven by aPAR. The variance in this relationship is mostly explained by the V_{cmax} and the chlorophyll content. This highlights the need for better treatment of chlorophyll content in biosphere models.
- The global and regional means as well as the zonal averages of both simulated Fs and GPP are in good agreement with the satellite-based F_s.
- The seasonality of the satellite-based F_s is quite well reproduced by the simulated F_s and GPP. However, the peaks of the simulated quantities lag by one month that of the satellite-based F_s in the Northern and Southern Hemispheres.
- A good agreement is found between the simulated F_s and computed GPP. The relationship is PFT dependent.
- A good agreement is found between the satellite-based F_s and the simulated quantities (F_s and GPP).

The study shows that the models of GPP and F_s in the CCDAS built around SCOPE do not allow us to propagate observations of F_s through constraint of V_{cmax} to improve estimates of GPP. For this version of CCDAS, this study would rather recommend the use of an empirical relationship between GPP and the satellite-based F_s, especially taking account of uncertainties in the radiation. Moreover, this empirical approach would be easier to implement and combined with other relevant data for the GPP would help to better estimate this quantity. However, a version of CCDAS which includes the full energy balance (including hydrological scheme) and prognostic photosynthesis (e.g., Knorr et al., 2010; Kaminski et al., 2013) and especially nitrogen scheme may give slightly different conclusion about the sensitivity of the fluorescence to V_{cmax}.

Acknowledgements. Rayner is in receipt of an Australian Professorial Fellowship (DP1096309). We are grateful to Christiaan van der Tol for providing the model SCOPE and his initial support.

References

Beer, C., Reichstein, M., Tomelleri, E., Ciais, P., Jung, M., Carvalhais, N., Rödenbeck, C., Arain, M. A., Baldocchi, D., Bonan, G. B., Bondeau, A., Cescatti, A., Lasslop, G., Lindroth, A., Lomas, M., Luyssaert, S., Margolis, H., Oleson, K. W., Roupsard, O., Veenendaal, E., Viovy, N., Williams, C., Woodward, F. I., and Papale, D.: Terrestrial gross carbon dioxide uptake: global distribution and covariation with climate, Science, 329, 834–838, 2010.

Berk, A., Anderson, G. P., Acharya, P. K., Chetwynd, J. H., Bernstein, L. S., Shettle, E. P., Matthew, M. W., and Adler-Golden, S. M.: MODTRAN4 User's Manual, Air Force Research Laboratory, Space Vehicles Directorate, Air Force Materiel Command, Hanscom AFB, MA 01731-3010, 97 pp., 2000.

Berry, J. A., Frankenberg, C., and Wennberg, P.: New Methods for Measurements of Photosynthesis from Space, KISS report, April, 2013.

Collatz, G. J., Ball, J. T., Grivet, C., and Berry, J. A.: Physiological and environmental regulation of stomatal conductance, photosynthesis and transpiration: a model that includes a laminar boundary layer, Agr. Forest Meteorol., 54, 107–136, 1991.

Collatz, G., Ribas-Carbo, M., and Berry, J. A.: Coupled photosynthesis-stomatal conductance model for leaves of C4 plants, Aust. J. Plant Physiol., 19, 519–538, 1992.

Evans, J. R.: Photosynthesis and nitrogen relationships in leaves of Ca plants, Oecologia, 78, 9–19, 1989.

BGD
12, 707–749, 2015

Farquhar, G., Von Caemmerer, S., and Berry, J.: A biochemical model of photosynthetic CO_2 assimilation in leaves of C3 species, Planta, 149, 78–90, 1980.
Frankenberg, C., Fisher, J. B., Worden, J., Badgley, G., Saatchi, S. S., Lee, J.-E., Toon, G. C., Butz, A., Jung, M., Kuze, A., Yokota, T.: New global observations of the terrestrial carbon cycle from GOSAT: patterns of plant fluorescence with gross primary productivity, Geophys. Res. Lett., 38, L17706, doi:10.1029/2011GL048738, 2011.
Frankenberg, C., O'Dell, C., Guanter, L., and McDuffie, J.: Remote sensing of near-infrared chlorophyll fluorescence from space in scattering atmospheres: implications for its retrieval and interferences with atmospheric CO_2 retrievals, Atmos. Meas. Tech., 5, 2081–2094, doi:10.5194/amt-5-2081-2012, 2012.
Genty, B., Birantais, J., and Baker, N.: The relationship between the quantum efficiencies of photosystems I and II in pea leaves, Biochim. Biophys. Acta, 990, 87–92, 1989.
Ghasemi, K., Ghasemi, Y., Ehteshamnia, A., Nabavi, S. M., Nabavi, S. F., Ebrahimzadeh, M. A., and Pourmorad, F.: Influence of environmental factors on antioxidant activity, phenol and flavonoids contents of walnut (*Juglans regia* L.) green husks, J. Med. Plants Res., 5, 1128–1133, 2011.
Gilmore, A. M. and Yamamoto, H. Y.: Dark induction of zeaxanthin-dependent non-photochemical fluorescence quenching mediated by ATP, P. Natl. Acad. Sci. USA, 89, 1899–903, 1992.
Gilmore, A. M., Mohanty, N., and Yamamoto, H. Y.: Epoxidation of zeaxanthin and antheraxanthin reverses nonphotochemical quenching of photo-system-II chlorophyll *a* fluorescence in the presence of trans-thylakoid delta-pH, FEBS Lett., 350, 271–274, 1994.
Guanter, L., Frankenberg, C., Dudhia, A., Lewis, P. E., G'omez-Dans, J., Kuze, A., Suto, H., and Grainger, R. G.: Retrieval and global assessment of terrestrial chlorophyll fluorescence from GOSAT space measurements, Remote Sens. Environ., 121, 236–251, 2012.
Hamazaki, T., Kaneko, Y., Kuze, A., and Kondo, K.: Fourier transform spectrometer for Greenhouse Gases Observing Satellite (GOSAT), Proc. SPIE, 73, 5659, doi:10.1117/12.581198, 2005.
Houborg, R., Cescatti, A., Migliavacca, M., and Kustas, W. P.: Satellite retrievals of leaf chlorophyll and photosynthetic capacity for improved modeling of GPP, Agr. Forest Meteorol., 177, 10–23, 2013.
Jacquemoud, S. and Baret, F.: PROSPECT: a model of leaf optical properties spectra, Remote Sens. Environ., 34, 75–91, 1990.

Joiner, J., Yoshida, Y., Vasilkov, A. P., Yoshida, Y., Corp, L. A., and Middleton, E. M.: First observations of global and seasonal terrestrial chlorophyll fluorescence from space, Biogeosciences, 8, 637–651, doi:10.5194/bg-8-637-2011, 2011.

Joiner, J., Yoshida, Y., Vasilkov, A. P., Middleton, E. M., Campbell, P. K. E., Yoshida, Y., Kuze, A., and Corp, L. A.: Filling-in of near-infrared solar lines by terrestrial fluorescence and other geophysical effects: simulations and space-based observations from SCIAMACHY and GOSAT, Atmos. Meas. Tech., 5, 809–829, doi:10.5194/amt-5-809-2012, 2012a.

Joiner, J., Yoshida, Y., Vasilkov, A. P., Middleton, E. M., Campbell, P. K. E., Yoshida, Y., Kuze, A., and Corp, L. A.: Filling-in of near-infrared solar lines by terrestrial fluorescence and other geophysical effects: simulations and space-based observations from SCIAMACHY and GOSAT, Atmos. Meas. Tech., 5, 809–829, doi:10.5194/amt-5-809-2012, 2012b.

Joiner, J., Guanter, L., Lindstrot, R., Voigt, M., Vasilkov, A. P., Middleton, E. M., Huemmrich, K. F., Yoshida, Y., and Frankenberg, C.: Global monitoring of terrestrial chlorophyll fluorescence from moderate-spectral-resolution near-infrared satellite measurements: methodology, simulations, and application to GOME-2, Atmos. Meas. Tech., 6, 2803–2823, doi:10.5194/amt-6-2803-2013, 2013.

Jung, M., Reichstein, M., Margolis, H. A., Cescatti, A., Richardson, A. D., Arain, M. A., Arneth, A., Bernhofer, C., Bonal, D., Chen, J., Gianelle, D., Gobron, N., Kiely, G., Kutsch, W., Lasslop, G., Law, B. E., Lindroth, A., Merbold, L., Montagnani, L., Moors, E. J., Papale, D., Sottocornola, M., Vaccari, F., Williams, C.: Global patterns of land–atmosphere fluxes of carbon dioxide, latent heat, and sensible heat derived from eddy covariance, satellite, and meteorological observations, J. Geophys. Res.-Biogeo., 116, G00J07, doi:10.1029/2010JG001566, 2011.

Kaminski, T., Knorr, W., Rayner, P., and Heimann, M.: Assimilating atmospheric data into a terrestrial biosphere model: a case study of the seasonal cycle, Global Biogeochem. Cy., 16, 1066, doi:10.1029/2001GB001463, 2002.

Kaminski, T., Giering, R., Scholze, M., Rayner, P., and Knorr, W.: An example of an automatic differentiation-based modelling system, in: Proceedings of the International Conference Computational Science – ICCSA 2003, Montreal, Canada, May 2003, edited by: Kumar, V., Gavrilova, L., Tan, C. J. K., and L'Ecuyer, P., Part II, volume 2668 of Lecture Notes in Computer Science, Springer, Berlin, 95–104, 2003.

Kaminski, T., Rayner, P. J., Voßbeck, M., Scholze, M., and Koffi, E.: Observing the continental-scale carbon balance: assessment of sampling complementarity and redundancy in a ter-

restrial assimilation system by means of quantitative network design, Atmos. Chem. Phys., 12, 7867–7879, doi:10.5194/acp-12-7867-2012, 2012.
Kaminski, T., Knorr, W., Schürmann, G., Scholze, M., Rayner, P. J., Zaehle, S., Blessing, S., Dorigo, W., Gayler, V., Giering, R., Gobron, N., Grant, J. P., Heimann, M., Hooker-Strout, A., Houweling, S., Kato, T., Kattge, J., Kelley, D., Kemp, S., Koffi, E. N., Köstler, C., Mathieu, P. P., Pinty, B., Reick, C. H., Rödenbeck, C., Schnur, R., Scipal, K., Sebald, C., Stacke, T., Terwisscha van Scheltinga, A., Vossbeck, Widmann, H., and Ziehn, T.: The BETHY/JSBACH carbon cycle data assimilation system: experiences and challenges, J. Geophys. Res., 118, 1414–1426, doi:10.1002/jgrg.20118, 2013, 2013.
Kattge, J., Knorr, W., Raddatz, T. J., and Wirth, C.: Quantifying photosynthetic capacity and its relationship to leaf nitrogen content for global-scale terrestrial biosphere models, Glob. Change Biol., 15, 976–991, doi:10.1111/j.1365-2486.2008.01744.x, 2009.
Knorr, W.: Annual and interannual CO_2 exchanges of the terrestrial biosphere: process-based simulations and uncertainties, Global Ecol. Biogeogr., 9, 225–252, 2000.
Knorr, W., Kaminski, T., Scholze, M., Gobron, N., Pinty, B., Giering, R., and Mathieu, P. P.: Carbon cycle data assimilation with a generic phenology model, J. Geophys. Res., 115, G04017, doi:10.1029/2009JG001119, 2010.
Koffi, E. N., Rayner, P., Scholze, M., and Beer, C.: Atmospheric constraints on gross primary productivity and net ecosystem productivity: results from a carbon-cycle data assimilation system, Global Biogeochem. Cy., 26, GB1024, doi:10.1029/2010GB003900, 2012.
Koffi, E. N., Rayner, P. J., Scholze, M., Chevallier, F., and Kaminski, T.: Quantifying the constraint of biospheric process parameters by CO_2 concentration and flux measurement networks through a carbon cycle data assimilation system, Atmos. Chem. Phys., 13, 10555–10572, doi:10.5194/acp-13-10555-2013, 2013.
Kuze, A., Suto, H., Nakajima, M., and Hamazaki, T.: Thermal and near infrared sensor for carbon observation Fourier-transform spectrometer on the Greenhouse Gases Observing Satellite for greenhouse gases monitoring, Appl. Optics, 48, 6716–6733, 2009.
Lee, J.-E., Frankenberg, C., van der Tol, C., Berry, J. A., Guanter, L., Boyce, C. K., Fisher, J. B., Morrow, E., Worden, J. R., Asefi, S., Badgley, G., and Saatchi, S.: Forest productivity and water stress in Amazonia: observations from GOSAT chlorophyll fluorescence, P. Roy. Soc. Lond. B Bio., 280, 20130171, doi:10.1098/rspb.2013.0171, 2013.
Le Quéré, C., Andres, R. J., Boden, T., Conway, T., Houghton, R. A., House, J. I., Marland, G., Peters, G. P., van der Werf, G. R., Ahlström, A., Andrew, R. M., Bopp, L., Canadell, J. G.,

BGD
12, 707–749, 2015

Ciais, P., Doney, S. C., Enright, C., Friedlingstein, P., Huntingford, C., Jain, A. K., Jourdain, C., Kato, E., Keeling, R. F., Klein Goldewijk, K., Levis, S., Levy, P., Lomas, M., Poulter, B., Raupach, M. R., Schwinger, J., Sitch, S., Stocker, B. D., Viovy, N., Zaehle, S., and Zeng, N.: The global carbon budget 1959–2011, Earth Syst. Sci. Data, 5, 165–185, doi:10.5194/essd-5-165-2013, 2013.

Maxwell, K. and Johnson, G. N.: Chlorophyll fluorescence – a practical guide, J. Exp. Bot., 51, 659–668, 2000.

Monteith, J. L.: Solar radiation and productivity in tropical ecosystems, J. Appl. Ecol., 9, 747–766, 1972.

Rayner, P., Scholze, M., Knorr, W., Kaminski, T., Giering, R., and Widmann, H.: Two decades of terrestrial Carbon fluxes from a Carbon Cycle Data Assimilation System (CCDAS), Global Biogeochem. Cy., 19, GB2026, doi:10.1029/2004GB002254, 2005.

Rosema, A., Snel, J. F. H., Zahn, H., Buurmeijer, W. F., and T. L., and Sampson, P. H.: Canopy Optical Indices van Hove, L. W. A.: The relation between laser- from infinite reflectance and canopy reflectance models induced chlorophyll fluorescence and photosynthesis, rem. for forest condition monitoring: application to hyperspec, Sens. Environ., 65, 143–154, 1998.

Scholze, M., Kaminski, T., Rayner, P., Knorr, W., and Giering, R.: Propagating uncertainty through prognostic carbon cycle data assimilation system simulations, J. Geophys. Res., 112, D17305, doi:10.1029/2007JD008642, 2007.

Seaton, G. G. and Walker, D. D.: Chlorophyll fluorescence as a measure of carbon metabolism, P. Roy. Soc. Lond. B Bio., 242, 29–35, 1990.

Shaahan, M. M., El-Sayed, A. A., and Abou El-Nour, E. A. A.: Predicting nitrogen, magnesium and iron nutritional status in some perennial crops using a portable chlorophyll meter, Sci. Hortic.-Amsterdam, 82, 339–348, 1999.

Su, Z., Timmermans, W. J., van der Tol, C., Dost, R., Bianchi, R., Gómez, J. A., House, A., Hajnsek, I., Menenti, M., Magliulo, V., Esposito, M., Haarbrink, R., Bosveld, F., Rothe, R., Baltink, H. K., Vekerdy, Z., Sobrino, J. A., Timmermans, J., van Laake, P., Salama, S., van der Kwast, H., Claassen, E., Stolk, A., Jia, L., Moors, E., Hartogensis, O., and Gillespie, A.: EAGLE 2006 – Multi-purpose, multi-angle and multi-sensor in-situ and airborne campaigns over grassland and forest, Hydrol. Earth Syst. Sci., 13, 833–845, doi:10.5194/hess-13-833-2009, 2009.

BGD

12, 707–749, 2015

Investigating the usefulness of satellite derived fluorescence data

E. N. Koffi et al.

van den Berg, A. K. and Perkins, T. D.: Evaluation of portable chlorophyll meter to estimate chlorophyll and nitrogen contents in sugar maple (*Acer saccharum* Marsh.) leaves, Forest Ecol. Manag., 200, 113–117, 2004.

van der Tol, C., Verhoef, W., and Rosema, A.: A model for chlorophyll fluorescence and photosynthesis at leaf scale, Agr. Forest Meteorol., 149, 96–105, 2009a.

van der Tol, C., Verhoef, W., Timmermans, J., Verhoef, A., and Su, Z.: An integrated model of soil-canopy spectral radiances, photosynthesis, fluorescence, temperature and energy balance, Biogeosciences, 6, 3109–3129, doi:10.5194/bg-6-3109-2009, 2009b.

van der Tol, C., Berry, J. A., Campbel, P. K. E., and Rascher, U.: Models of fluorescence and photosynthesis for interpreting measurements of solar induced chlorophyll fluorescence, J. Geophys. Res. Biogeosci., 119, doi:10.1002/2014JG002713, 2014.

Verhoef, W. and Bach, H.: Coupled soil-leaf-canopy and atmosphere radiative transfer modeling to simulate hyperspectral multi-angular surface reflectance and TOA radiance data, Remote Sens. Environ., 109, 166–182, 2007.

Verhoef, W., Jia, L., Xiao, Q., and Su, Z.: Unified optical-thermal four-stream radiative transfer theory for homogeneous vegetation canopies, IEEE T. Geosci. Remote, 45, 1808–1822, 2007.

Verhoef, W., van der Tol, C., and Middleton, E. M.: Vegetation canopy fluorescence and reflectance retrieval by model inversion using optimization, in: 5th International Workshop on Remote Sensing of Vegetation Fluoresence, 22–24 April 2014, Paris, France, available at: http://www.congrexprojects.com/2014-events/14c04/proceedings, 2014.

von Caemmerer, S. and Farquhar, G. D.: Some relationships between the biochemistry of photosynthesis and the gas exchange of leaves, Planta, 153, 376–387, 1981.

Wilson, M. F. and Henderson-Sellers, A.: A global archive of land cover and soil data for use in general circulation climate models, J. Climatol., 5, 119–143, 1985.

Weedon, G. P., Gomes, S., Viterbo, P., Shuttleworth, W. J., Blyth, E., Österle, H., Adam, J. C., Bellouin, N., Boucher, O., and Best, M.: Creation of the WATCH forcing data and its use to assess global and regional reference crop evaporation over land during the twentieth century, J. Hydrometeorol., 12, 823–848, 2011.

Zhang, Y., Guanter, L., Berry, J. A., Joiner, J., van der Tol, C., Huete, A., Gitelson, A., Voigt, M., and Köhler, P.: Estimation of vegetation photosynthetic capacity from space-based measurements of chlorophyll fluorescence for terrestrial biosphere models, Glob. Change Biol., 20, 3727–3742, doi:10.1111/gcb.12664, 2014.

Table 1. Main controlling parameters for the photosynthesis and fluorescence models are given. V_{cmax} stands for carboxylation maximum capacity and C_{ab} for the chlorophyll content AB for 13 plant functional types (PFT) as used in the CCDAS.

PFT number	Plant Function Type (PFT)	V_{cmax} (µmol (CO_2) m^{-2} s^{-1}) Prior value	Optmized values Koffi et al. (2012)	C_{ab} (µg cm^{-2})
1	Tropical broadleaved evergreen tree	60	63.8	40
2	Tropical broadleaved deciduous tree	90	73.5	15
3	Temperate broadleaved evergreen tree	41	39.7	15
4	Temperate broadleaved deciduous tree	35	149.2	10
5	Evergreen coniferous tree	29	21.9	10
6	Deciduous coniferous tree	53	136.4	10
7	Evergreen shrub	52	168.9	10
8	Deciduous shrub	160	96.1	10
9	C3 grass	42	18.9	10
10	C4 grass	8	0.7	5
11	Tundra	20	8.5	10
12	Swamp	20	9.3	10
13	Crop	117	47.9	20

BGD
12, 707–749, 2015

Investigating the usefulness of satellite derived fluorescence data

E. N. Koffi et al.

Table 2. Set ups for the CCDAS simulations based on the carboxylation maximum capacity (V_{cmax}) and chlorophyll content AB (C_{ab}) are given. The values of prior and optimized V_{cmax} as well as C_{ab} PFT-specific are given in Table 1. The constant value of C_{ab} for all the 13 PFTs is set to 40 $\mu g\,cm^{-2}$.

Model configuration	V_{cmax}	C_{ab}
S1	Prior values	Constant value for all the 13 PFTs
S2	Prior values	C_{ab} PFT-specific
S3	Optimized values	Constant value for all the 13 PFTs
S4	Optimized values	C_{ab} PFT-specific

BGD
12, 707–749, 2015

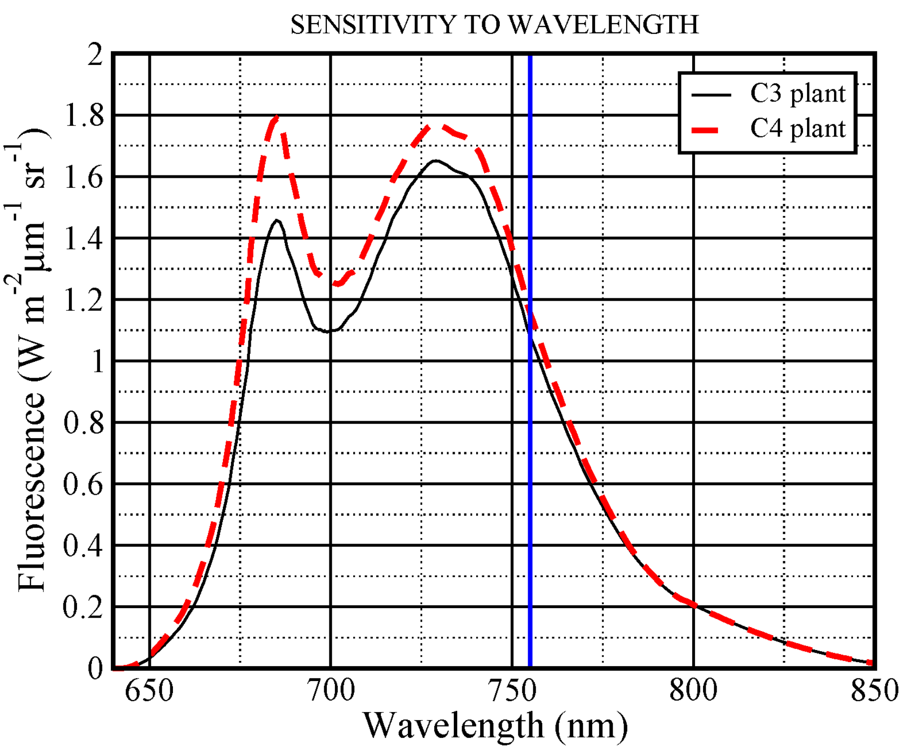

Figure 1. The simulated fluorescence at the top of the canopy as a function of the incoming radiation wavelength and for C3 (black solid line) and C4 (red dashed line) plants from the model SCOPE are shown, respectively. The blue solid line corresponds to wavelength value (i.e., 755 nm) at which the simulated F_s is calculated in this study, i.e., the equivalent of the satellite GOSAT based F_s.

BGD
12, 707–749, 2015

BGD
12, 707–749, 2015

Investigating the usefulness of satellite derived fluorescence data

E. N. Koffi et al.

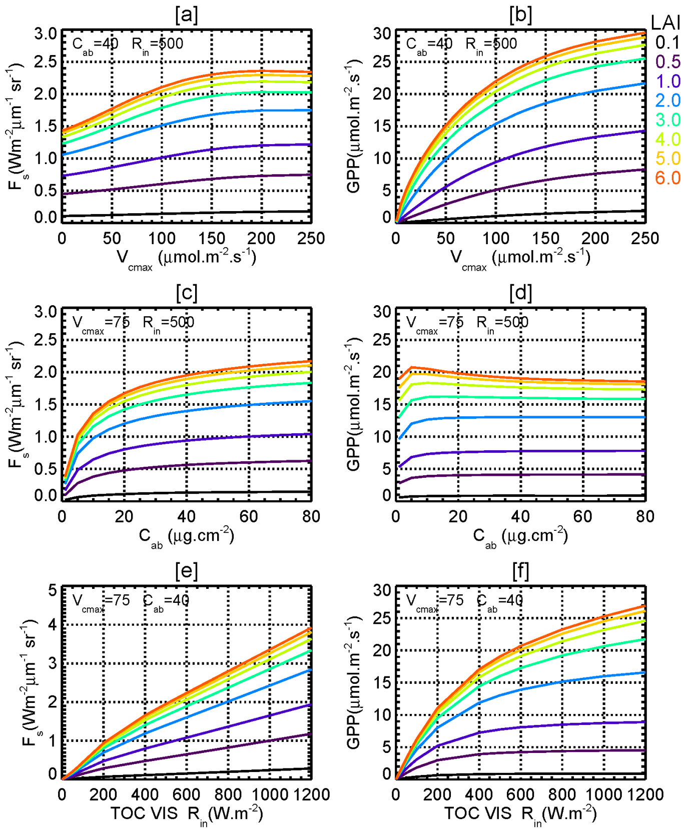

Figure 2. The sensitivities of SCOPE fluorescence (F_s) at the top of the canopy (TOC) of C_3 plant to the carboxylation maximum capacity (V_{cmax}), chlorophyll content AB (C_{ab}), and to TOC visible radiation (TOC VIS R_{in}) for several leaf area index (LAI) are shown. Graphs (**a** and **b**) stand for F_s and GPP as function of V_{cmax}, respectively. The graphs (**c** and **d**) give the sensitivities of F_s and GPP to C_{ab}, respectively. The graphs (**e** and **f**) show F_s and GPP as a function of short wave radiation at the TOC (R_{in}), respectively.

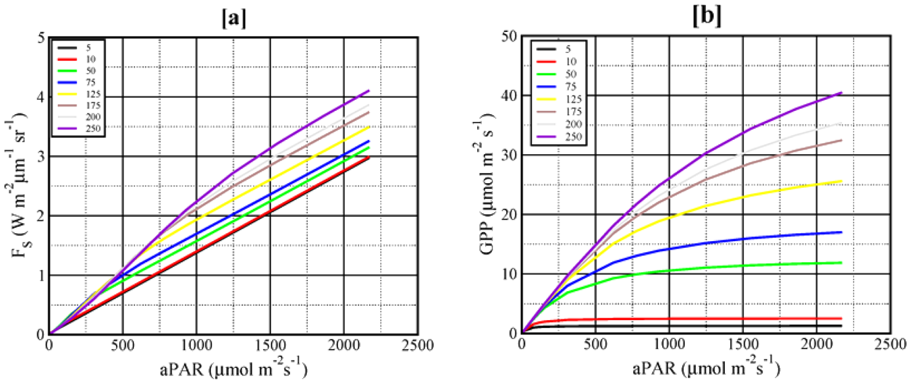

Figure 3. The sensitivities of the SCOPE fluorescence F_s **(a)** and gross primary productivity (GPP) **(b)** to the absorbed photosynthetically active radiation (aPAR) and for several V_{cmax} are presented. LAI is set to 2. Results from a C_3 plant are shown.

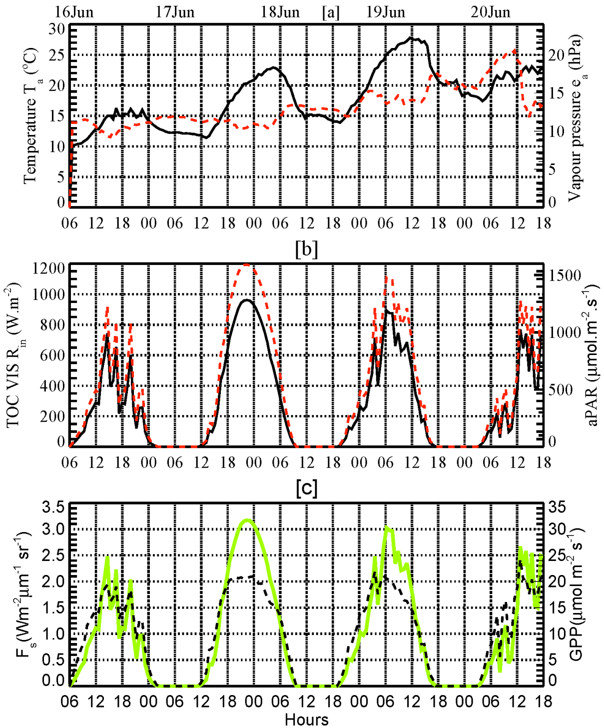

Figure 4. SCOPE simulations of fluorescence F_s, gross primary productivity (GPP), and absorbed photosynthetically active radiation (aPAR) from in situ measurements obtained during 16 June to 20 June 2006 period over a canopy located at 52.25 deg latitude and 5.69 deg longitude in the Netherlands are shown. The graph **(a)** presents the temporal variations of the temperature (black solid) and the vapour pressure (dashed red line). The graph **(b)** gives the temporal variations of the observed visible radiation of both the top of canopy (TOC VIS R_{in}: black solid line) and the computed aPAR (dashed red line). The graph **(c)** shows the temporal variations of both SCOPE F_s (solid green line) and GPP (black dashed line). The C_3 plant is considered.

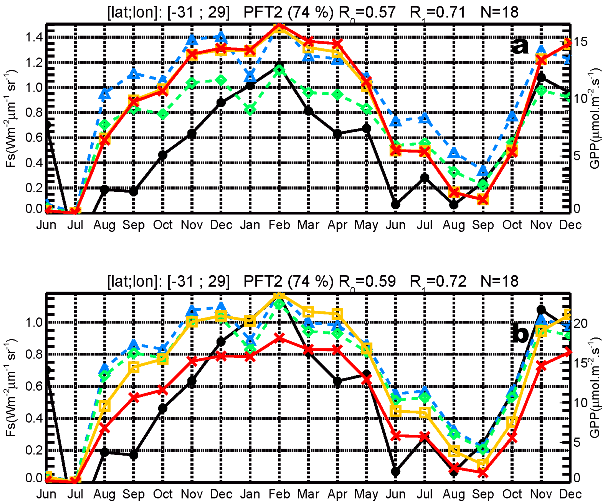

Figure 5. Temporal variations (June 2009 to December 2010) of CCDAS simulations of the fluorescence F_s and GPP for different values of the carboxylation maximum capacity (V_{cmax}) and the chlorophyll AB content (C_{ab}) and for a plant functional type (PFT 2: Tropical broadleaved evergreen tree) are show. In the graphs (**a** and **b**), the satellite GOSAT based F_s is shown in black solid line with big dot.
In the graph **(a)**, two simulated F_s are shown: F_s (blue dashed line with triangles) and GPP (orange solid line with rectangles) by using C_{ab} value of 40 µg cm^{-2}, respectively. F_s (green dashed line with diamond) and GPP (orange solid line with rectangle triangles) by using C_{ab} value of 15 µg cm^{-2}, respectively. For this last set up, the correlation coefficient R_0 between simulated F_s and satellite based F_s is given.
In graph **(b)**, simulations are: F_s (blue dashed line with triangle) and GPP (orange solid line with rectangle) are obtained by using the prior V_{cmax} of 90 µmol (CO_2) m^{-2} s^{-1}, respectively. F_s (blue dashed line with diamonds) and GPP (red solid line with crosses) are calculated by using the optimized V_{cmax} of 73.5 µmol (CO_2) m^{-2} s^{-1}, respectively. For this last set up, the correlation coefficient R_1 between simulated GPP and satellite based F_s is given.

BGD
12, 707–749, 2015

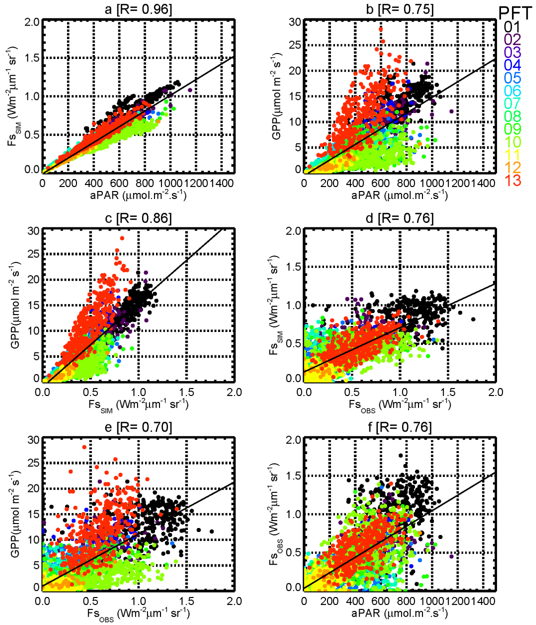

Figure 6. Correlations between CCDAS simulated quantities and between simulated quantities and satellite GOSAT based fluorescence F_s are shown. The graph **(a)** presents the correlation between CCDAS simulated F_s ($F_{s_{SIM}}$) and the simulated absorbed photosynthetically active radiation (aPAR). The graph **(b)** shows the gross primary productivity (GPP) as function of aPAR. The graph **(c)** displays the correlation between GPP and simulated F_s. The graph **(d)** presents the correlation between simulated F_s ($F_{s_{SIM}}$) and the satellite based F_s ($F_{s_{OBS}}$). The graph **(e)** displays GPP as function of $F_{s_{OBS}}$. The graph **(f)** shows $F_{s_{OBS}}$ as a function of aPAR. The dominant plant functional types (PFT) characterizing by the PFTs having at least 50 % of the spatial coverage for the pixels of the CCDAS at the spatial resolution of $2^\circ \times 2^\circ$ (longitude × latitude) are shown by different colors. The number of pair of data is 2857. The Pearson coefficient of the linear correlation R is indicated. Data for June 2009 to December 2010 period are considered.

BGD
12, 707–749, 2015

Investigating the usefulness of satellite derived fluorescence data

E. N. Koffi et al.

BGD
12, 707–749, 2015

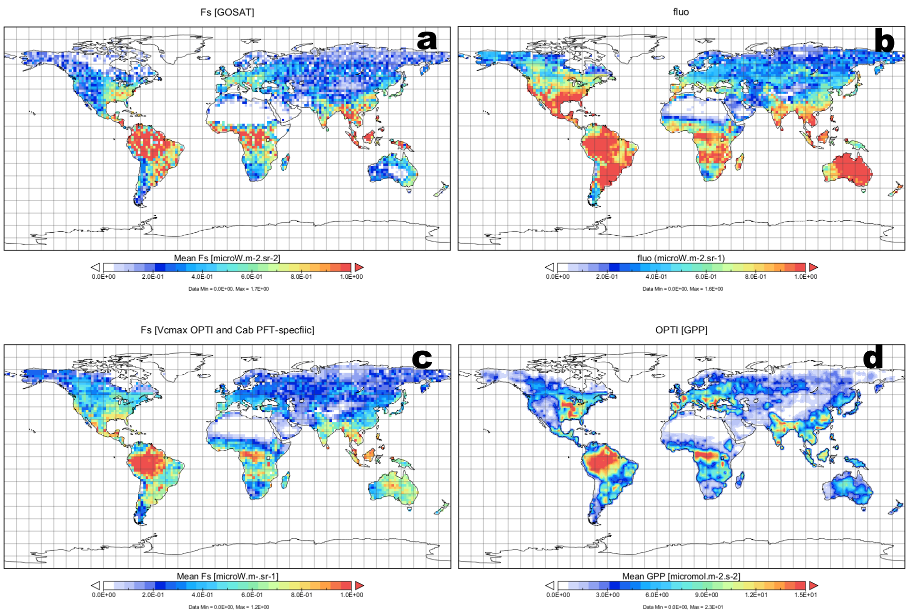

Figure 7. Mean spatial patterns over the year 2010 of **(a)** satellite GOSAT based fluorescence F_s, **(b)** CCDAS simulated F_s by using constant value of the chlorophyll content AB C_{ab} for all the 13 PFTs (setting S3 in Table 2), **(c)** C_{ab} PFT specific (setting S4 in Table 2) are shown. The graph **(d)** displays the mean spatial patterns of the gross primary productivity (GPP) by using both C_{ab} PFT specific and optimized carboxylation maximum capacity (V_{cmax}) (setting S4 in Table 2).

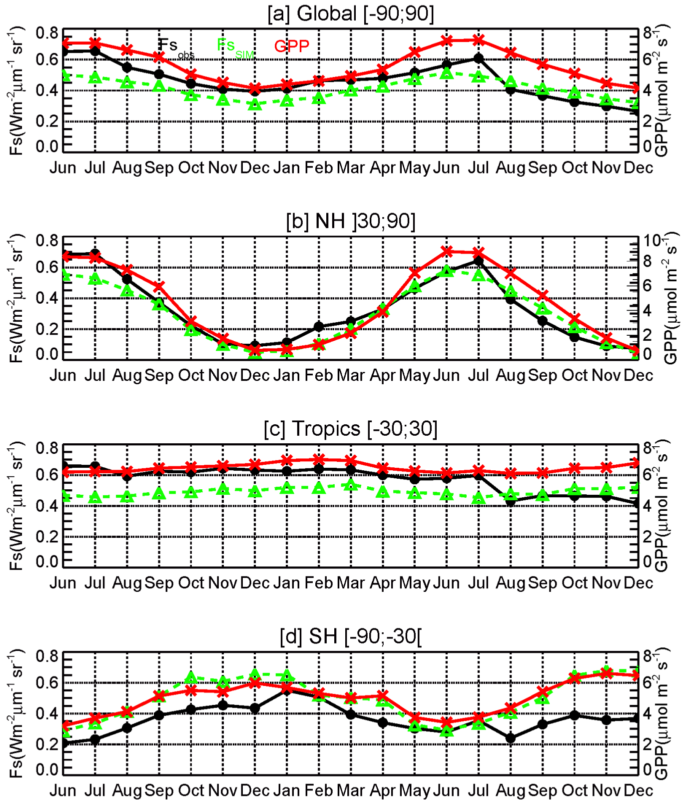

Figure 8. Global **(a)** and regional (**b** to **d**) means of fluorescence F_s and gross primary productivity GPP over June 2009 to December 2010 period are shown. The satellite GOSAT based F_s ($F_{s_{OBS}}$: black solid line with big dot), simulated F_s ($F_{s_{SIM}}$: green dashed line with triangles), and the simulated gross primary productivity (GPP: red solid line with crosses) are displayed. The CCDAS set up S4 (Table 2) is considered.

BGD
12, 707–749, 2015

Title Page
Abstract | Introduction
Conclusions | References
Tables | Figures
◀◀ | ▶▶
◀ | ▶
Back | Close
Full Screen / Esc
Printer-friendly Version
Interactive Discussion

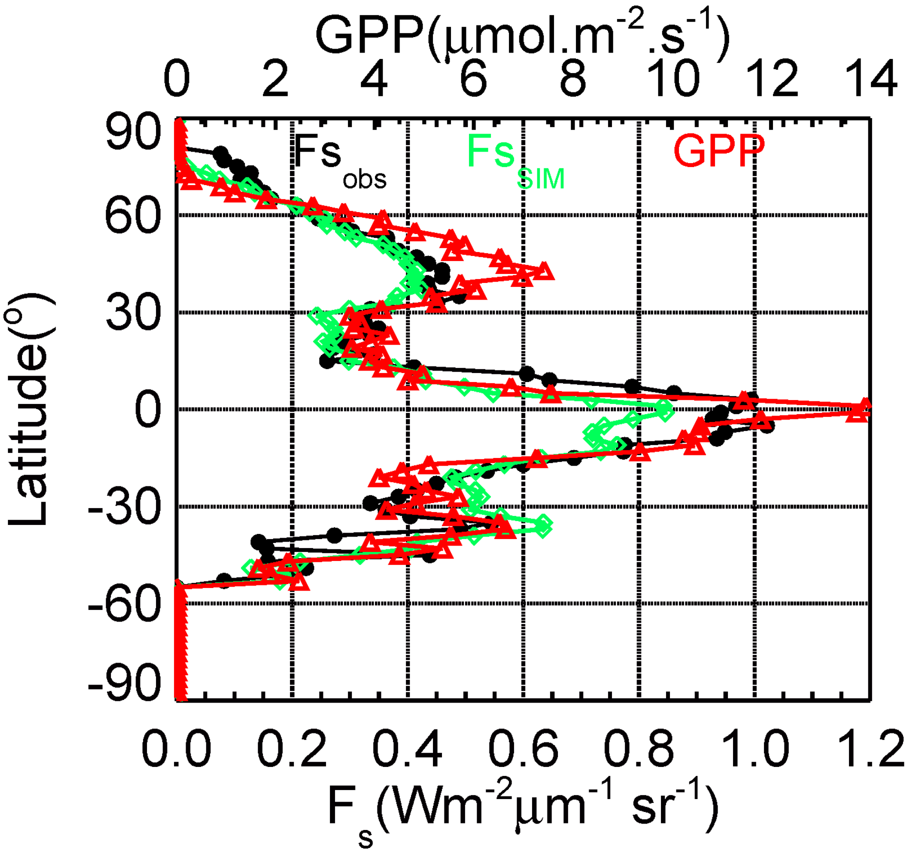

Figure 9. Latitudinal distributions of the satellite GOSAT based F_s ($F_{s_{OBS}}$: black solid line with big dot), simulated F_s ($F_{s_{SIM}}$: green solid line with diamonds), and gross primary productivity (GPP: red solid line with triangles) within 5° latitudinal band are shown. The CCDAS set up S4 (Table 2) is considered. The period of June 2009 and December 2010 period is considered.

BGD
12, 707–749, 2015

Investigating the usefulness of satellite derived fluorescence data

E. N. Koffi et al.